PEA-15 Engages in Allosteric Interactions Using a Common Scaffold in a Phosphorylation-Dependent Manner

Joyce Ikedife
New Jersey City University
Jianlin He
Third Institute of Oceanography
Yufeng Wei (ywei@njcu.edu)
New Jersey City University

Research Article

Keywords: PEA-15 , Allosteric Interactions, Common Scaffold, Phosphorylation-Dependent Manner

Posted Date: September 13th, 2021

DOI: https://doi.org/10.21203/rs.3.rs-870954/v1

Version of Record: A version of this preprint was published at Scientific Reports on January 7th, 2022.
See the published version at https://doi.org/10.1038/s41598-021-04099-6.

Abstract

Phosphoprotein enriched in astrocytes, 15 kDa (PEA-15) is a death-effector domain (DED) containing protein involved in regulating mitogen-activated protein kinase and apoptosis pathways. In this molecular-dynamics study, we examined how phosphorylation of the PEA-15 C-terminal tail Ser-104 and Ser-116 allosterically promotes conformational changes of the DED, and alters the binding specificity from extracellular-regulated kinase (ERK) to Fas associated death domain (FADD) protein. We found that the binding interfaces between the unphosphorylated PEA-15 and ERK2 and the doubly phosphorylated PEA-15 and FADD are similarly composed of a scaffold that includes both the DED and the C-terminal tail of PEA-15. While the unphosphorylated serine residues do not directly interact with ERK2, the phosphorylated Ser-116 engages in strong interactions with arginine residues on FADD DED. In this DED complex, FADD repositions its death domain (DD) relative to the DED, which has strong implications on the association of the death-inducing signaling complex (DISC).

Introduction

Phosphorylation is arguably the most prevalent posttranslational modification that could completely alter the fate of the cell. Excessive phosphorylation in cells could be cancerous, while sublevel phosphorylation makes the cells more susceptible to unnecessary cell death. As we proposed earlier, a delicate balance of phosphorylation level inside cells must be vigorously maintained in order to keep the cells at optimal conditions, which we have termed phosphorylation homeostasis[1]. Here we report our computational studies on a small, non-catalytic protein, phosphoprotein enriched in astrocytes, 15 kDa (PEA-15), which engages in a phosphorylation-mediated conformational modulation that completely switches the binding specificity of the protein and regulatory pathways, and subsequently determines the cell fate.

First identified in astrocytes as a substrate for protein kinase C (PKC)[2], PEA-15 was found to be ubiquitously expressed in all types of cells and tissues, and is highly conserved among mammals[3]. PEA-15 has no catalytic activity, but it plays a significant role in regulating both cell proliferation and apoptosis (programmed cell death) through interacting with either the mitogen-activated protein (MAP) kinases, extracellular signal-regulated kinases (ERK) 1 and 2, or Fas-associated via death domain (FADD) protein. Structurally, PEA-15 consists a canonical six-helix bundled death-effector domain (DED) at the N-terminus, and a long, irregularly structured C-terminal tail[4,5]. While the C-terminal tail is intrinsically disordered, it is evident that the C-terminal tail is crucial in ERK binding [4,6,7], and it contains the two phosphorylation sites, Ser-104, substrate for PKC [2,8], and Ser-116, substrate for protein kinase B/Akt[9] and Ca^{2+}-calmodulin dependent protein kinase II (CaMKII)[8]. Unphosphorylated PEA-15 interacts with ERK1/2, preventing ERK1/2 from translocating into the nucleus due to the presence of a nuclear exporting sequence (NES), and blocking ERK-dependent transcription and proliferation[10]. Double phosphorylation at both serine residues (*p*-S104/*p*-S116) alters the binding specificity of PEA-15 from ERK1/2 to FADD, preventing the recruitment and activation of procaspase-8 at the death-inducing signaling complex (DISC), and blocking death receptor-initiated apoptosis[11–13]. Specifically, *p*-S104 blocks the interaction

with ERK, and *p*-S116 promotes the recruitment of PEA-15 to the DISC *in vivo*[14]. In other words, unphosphorylated PEA-15 is a tumor suppressor as it inhibits ERK-dependent proliferation, while the doubly phosphorylated protein becomes a tumor promotor as it blocks apoptosis[15]. PEA-15 phosphorylation fits very well into the hallmark of almost all tumors in that it promotes unrestricted proliferation and inhibit apoptosis[1]. It is still unclear, however, how phosphorylation at an intrinsically disordered region of PEA-15 could completely switch the binding specificity from one protein to another.

To answer these questions, we conducted molecular dynamics (MD) simulations on the free PEA-15, the doubly phosphorylated *p*-S104/*p*-S116 PEA-15 (PEA-15pp), and the complexes between unphosphorylated PEA-15 and ERK2, and PEA-15pp and FADD. Here we report an conformational control mechanism mediated by the phosphorylation on the C-terminal tail, and a common scaffold on PEA-15 in the interactions with both ERK2 and FADD. The binding specificity is allosterically controlled by the charge-charge interactions involving phosphorylation on Ser-116. We also report, for the first time, a DED complex in the PEA-15pp/FADD interacting model, which highlights a potential mode for DED-DED interactions. This DED complex model provides significant insights into the formation of the DISC and the activation of the extracellular receptor-initiated apoptosis pathway.

Results

Structures and conformations of unphosphorylated and phosphorylated PEA-15

For unphosphorylated PEA-15 and phosphorylated PEA-15pp proteins in their free forms, 50-ns MD simulations were performed. The root-mean-square deviation (RMSD) plots for both PEA-15 and PEA-15pp simulations indicated that the structures reached equilibrium after 30 ns. The large fluctuation in RMSD was due to the intrinsically disordered C-terminal tail, while the DED displayed relatively small RMSD (Supplementary Figure S1). The subsequent analyses were performed using the last 20 ns of the simulations for both PEA-15 and PEA-15pp. The disordered nature of the C-terminal tail in both unphosphorylated and phosphorylated free-form proteins is clearly visible from the per-residue root-mean-square fluctuation (RMSF) analyses (Supplementary Figure S2), with RMSF values for the C-terminal tail much higher than those of the DED, indicating high flexibility and elevated motion of the disordered tail.

The simulated structure of the unphosphorylated PEA-15 closely resembles the experimental NMR structure (PDB ID 2LS7), with the backbone RMSD between the simulated and experimental DED structures of 1.499 Å (Fig. 1A). Although the simulated PEA-15pp structure largely maintained a six-helix bundle fold, the phosphorylation at the C-terminal serine residues caused some important changes from the unphosphorylated protein (Fig. 1B). Most remarkably, the α3 helix shifts considerably from the unphosphorylated structure, and the α6 helix exhibits a kink at residue Arg-85 in the phosphorylated structure. The backbone RMSD of the DED residues between PEA-15pp and experimental

unphosphorylated structure is 2.027. The overlay of simulated PEA-15 and PEA-15pp structures shows the same distinction, with backbone RMSD of DED residues of 1.994 Å (Fig. 1C).

Complex structure of unphosphorylated PEA-15 with ERK2

For the two complexes formed between unphosphorylated PEA-15 with ERK2 (PEA-15/ERK2) and between phosphorylated PEA-15pp with FADD (PEA-15pp/FADD), 150-ns MD simulations were performed. The simulations for the two complexes stabilized at after 100 ns (Supplementary Figure S3). The analyses for these two complexes were conducted using the last 50-ns trajectories. In these complexes, it is noticeable from the RMSF plots that the PEA-15 protein greatly reduces the motion and flexibility in the C-terminal tail comparing to the free-form proteins due to the strong interaction between the tail and the interacting proteins (Supplementary Figure S4). In the PEA-15/ERK2 complex, tail residues 121–129 tightly bind to ERK D-peptide recruitment site (DRS), resulting in significant immobilization in the region[7,16]. In the PEA-15pp/FADD complex, the phosphorylated p-S116 interacts strongly with R34 and R38 on FADD (see below), stabilizing the tail in the complex.

In the PEA-15/ERK2 complex structure (Fig. 2A), the PEA-15 protein exhibit large conformational change in the DED, particularly at helix α3, which is completely uncoiled. Helices α2 and α4 also display slight shifts from their free-form position. Helices α1, α5, and α6 are mostly maintained their positions. The backbone RMSD of PEA-15 DED between the complex and the free-form is 2.734 Å. The unwinding of the α3 helix is consistent with previous experimental results, including our NMR dynamics study, which indicated an increased dynamics in this region[7], the X-ray crystallography study of PEA-15/ERK2 complex structures, in which no electron density could be observed in this region[16], and our CS-Rosetta model of PEA-15 in the complex, which also characterized helix α3 as disordered[17].

The ERK2 structure in the simulated PEA-15/ERK2 complex does not exhibit much difference from the initial structure derived from crystal structure 4IZ5, with backbone RMSD of 2.002 Å (Fig. 2B). Most of the variations are localized in the loop regions, while the regular secondary structural components remain mostly intact, indicating a relatively rigid ERK2 in the complex. The per-residue RMSF is relatively small (< 0.3 Å) throughout the ERK2 sequence, with the exception of the activation loop preceding the phosphorylation sites of Thr185 and Tyr187, and a long loop near the end of C-lobe of ERK2 (Supplementary Figure S5).

Complex structure of phosphorylated PEA-15pp binding with FADD

FADD is comprised of an N-terminal death effector domain (DED) and a C-terminal death domain (DD) followed by a short tail. It is the adapter protein between the DD-containing death receptor, Fas, and the DED-containing procapspase-8, promoting the formation of the death-inducing signaling complex (DISC) through specific homotypic domain-domain interactions[18]. In the PEA-15pp/FADD complex structure, the phosphorylated PEA-15pp doesn’t seem to undergo additional conformational change in the DED from the free-form structure, with the exception of the kink at the end of the helix α6 (Fig. 3A). The backbone

RMSD for PEA-15pp DED (before the kink) is only 0.803 Å between the free and FADD-bound structures. The simulation results of PEA-15pp in its free and FADD-bound form are consistent with our earlier NMR data, which indicated that phosphorylation at S104 and S116, mimicked by serine to aspartic acid mutation, on the C-terminal tail stimulates a conformational change at the DED, and FADD binding does not induce additional changes in DED conformation[17]. The NMR data and the current MD simulations both suggest that phosphorylation of C-terminal serine residues is enough to modulate the DED structure, converting the protein conformation better suited to bind with FADD.

PEA-15pp and FADD engage in canonical homotypic interactions within death superfamily proteins[19], and the two proteins bind to each other using their respective DED surfaces. Currently, there have not been any experimental DED complex structures reported, and our PEA-15pp/FADD model provides a first snapshot of a DED complex. The binding surface on PEA-15pp is located at helices α5/α6 of the DED, and the surface on FADD is located at helices α1/α6 of the DED. The orientations of the two interacting DEDs are orthogonal to each other (Fig. 3B).

The FADD structure exhibits significant changes upon PEA-15pp binding. The FADD DED in the complex does not show much change from the free FADD (PDB ID 2GF5), with backbone RMSD between the bound and free forms of 2.118 Å. The death domain (DD) on FADD showed much larger conformational change, involving the reorientation of helices α2, α3, and α4 relatively to the other three helices, with backbone RMSD between the bound and free structures of 3.447 Å. The most remarkable change in FADD structure can be observed when the DEDs in the free and bound forms are superimposed, illustrating that the DD is shifted towards PEA-15pp in the bound structure, rotating about 90° relative to the DED around the flexible linker between the two domains (Figs. 3B and 3C). The relative reorientation between the two domains will have significant implication in the DISC formation, as discussed in the next section.

Surface polar interactions on PEA-15

On PEA-15, and most other DED-containing proteins, three charged amino acids, D19-R72-D74, form an electrostatic and hydrogen-bonded network, termed charge-triad. The distances between these three residues, however, are not consistent among different states of PEA-15 (Supplementary Figure S6). The simulations showed that for free-form PEA-15, D19-R72 interaction is more consistent despite small fluctuations over time, while R72-D74 distance is general quite large and has no close contact. Upon phosphorylation at the C-terminal tail serine residues, D19-R72 interaction becomes even more uniform, and R72-D74 distance closes up with relatively small fluctuations. In the PEA-15/ERK2 complex, R72-D74 interaction becomes increasingly uniform with little fluctuation, while D19-R72 interaction is destabilized. Same trend can be observed for PEA-15pp/FADD complex, in which R72-D74 distance is very consistent with virtually no fluctuation, while D19-R72 interaction is less stable comparing to free PEA-15pp. Generally, free-forms of PEA-15 favor D19-R72 interaction, while the bound-forms favor R72-D74 interaction. Phosphorylation at PEA-15 C-terminal tail is sufficient to bring R72-D74 distance closer, and FADD binding completely stabilizes R72-D74 interaction.

In addition to the charge triad, there are numerous other polar interactions (electrostatic and hydrogen bonding) on the surface of the PEA-15 in the free forms and complexes. The patterns of the polar interactions, however, vary depending on the phosphorylate states and binding of protein partners. A list of these polar interactions on PEA-15 surface is available in the Supplementary Table S1. The only non-charge-triad interaction consistently observed in all models is the one between Glu-21 and Lys-24. Other interactions identified in the DED of unphosphorylated free-form protein include Y4-E50, D30-Y62, K35-E38, E64-R83. Most of these interactions are broken when the conformational change is induced by phosphorylation, and new interactions are formed, including N14-R72, T16-D19, D30-K54, N59-S61. Upon binding to ERK2, many of the original interactions in the free-form are also broken, and a new interaction between D81-R85 is formed. The phosphorylated PEA-15pp has kept some of the same interactions in the FADD complex, indicating a less extensive conformational change switching from the free form to the bound form. Most of the shifts in polar interactions are at the binding interface, as described in the next section. The changes of these polar interactions facilitate the conformational changes by reducing the transition energies between conformations.

Binding interfaces in PEA-15/ERK2 and PEA-15pp/FADD complexes

The two binding interfaces between PEA-15 and ERK2 revealed in this MD study are consistent with earlier crystal structures[16]. PEA-15 utilizes its helices α5 and α6 of the DED to interact with the docking site for ERK, FxF (DEF) of ERK2, and uses its C-terminal tail to interacts with the D-peptide-recruitment site (DRS, also termed as DEJL, or docking site for ERK and JNK, LXL or kinase interaction motif) of ERK2. PEA-15 DED residue Arg-71 on the loop between helices α5 and α6 are directly involved in binding to DEF site residue Tyr-205 (Fig. 4A), while the charge-triad residues (D19, R72, and D74) do not directly involved in binding to ERK2. PEA-15 C-terminal residues 121–129 interact with the ERK2 DRS residues as it contains a reversed pseudo-D-peptide sequence (Fig. 4B)[20,21]. Particularly, Lys-128 on the PEA-15 C-terminus directly interacts with Asp-124 of ERK DRS. The C-terminal residues 101–110 also exhibit significant interactions with ERK2, including the interaction between Asp-110 of PEA-15 and Arg-225 of ERK2, although it is a relatively flexible region as the RMSF values in this region are relatively high (Supplementary Figure S4), and this part of the protein did not produce electron density in the crystal structures. The atomic distances of these intermolecular interactions are plotted in Supplementary Figure S7A. All distances seemed to be stabilized after 120 ns of simulation. It is worth noting that the two phosphorylation sites, Ser-104 and Ser-116, of PEA-15 are not directly involved in the interaction of ERK2, which may explain the observation that phosphorylation states of PEA-15 do not affect the binding affinity with ERK2 *in vitro*[21].

Our PEA-15pp/FADD complex model provided a novel insight into the DED-DED interacting mode. The binding interface between the two DEDs is composed of residues from helix α5 and α6 of PEA-15pp, and residues on helices α1 and α6 of FADD DED. The two DEDs are arranged perpendicular to each other. Arg-71, located on the loop between helices α5 and α6 of PEA-15pp, is directly hydrogen bonded to Asp-81, located on helix α6 of the FADD DED (Fig. 5A). It is worth noting that Arg-71 also engages in interaction

with ERK2 as discussed earlier. The C-terminal tail residues of PEA-15pp interact with residues on helices α3 and α4 of the FADD DED, including strong electrostatic and hydrogen-bonding interactions between phosphor-Ser-116 on PEA-15pp and Arg-34 and Arg-38 on helix α3 of FADD DED, and the interaction between Arg-101 of PEA-15pp and Glu-51 on helix 4 of FADD DED (Fig. 5B). The atomic distances of these intermolecular interactions are plotted in Supplementary Figure S7B. The Arg-71 of PEA-15 has relatively stable interaction with Asp-81 of FADD throughout the simulation, although there are some fluctuations at certain timepoints. The interactions between the phosphorylated Ser-116 of PEA-15 and the two arginine residues on FADD seemed to be stabilized early on at around 100 ns. The pS116 interactions may have helped the formation of other intermolecular interactions, particularly for the C-terminal tail residues, such as Arg-101, which only shows stable interaction with Glu-51 of FADD after around 140 ns. The direct involvement of phosphor-Ser-116 to interact with FADD positively charged arginine residues may provide an insight on how phosphorylation of PEA-15 modulates its binding specificity *in vivo*. Unphosphorylated PEA-15, which has neutral charge on Ser-116, cannot engage in strong electrostatic interactions with the positive arginine patch on FADD, will tend to bind to ERK1/2. The phosphorylated PEA-15pp, in which the negative charge on pSer-116 engages in strong electrostatic interactions with FADD to facilitate the involvement of other intermolecular interactions between the two molecules, will tend to bind to FADD.

The pairwise mean-smallest-distance maps illustrate these interactions (Supplementary Figure S8). In the intermolecular region on the PEA-15/ERK2 map, short distances can be observed in both the α5/α6 – DEF site and the C-terminal tail – DRS interactions. Similarly, in the PEA-15pp/FADD interaction map, short distances can be observed in the PEA-15 α5/α6 interaction with FADD DED α1/α6, as well as the PEA-15 C-terminal tail interaction with the α3/α4 of the FADD DED. Additionally, the FADD C-terminal tail interacts with PEA-15 α1 and α6. As expected, there are essentially no interactions between PEA-15 DED and FADD DD.

The interactions between both PEA-15 and ERK2 and PEA-15pp and FADD are largely electrostatic, as shown on the electrostatic potential surfaces (EPS) of the complexes (Fig. 6). The PEA-15 surface on the helices 5 and 6, used for interacting with both ERK2 and FADD, is primarily negatively charged, while both the ERK2 DEF binding site and FADD α1/α6 surface are mainly positively charged. The binding mode at the PEA-15 C-terminal tail is more complicated. In the PEA-15/ERK2 interaction, PEA-15 utilizes its pseudo-D-peptide sequence at the end of the tail, which consists of several lysine residues and is highly positively charged, to interact with ERK2 DRS, which contains mostly negatively charged amino acids (Asp and Glu). In the PEA-15pp/FADD complex, the main interaction is the one between the pSer-116, which is highly negatively charged, and the positive patch with arginine residues on helix 3 of the FADD DED. Another major interaction between PEA-15pp and FADD is located between the negative charge on helix 1 of PEA-15pp and the positive charge of the FADD tail.

Discussion

As a versatile regulatory protein ubiquitously expressed in almost all mammalian cell types and tissues, PEA-15 controls multiple biological processes in a phosphorylation-dependent manner. The protein itself, however, does not seem to have any dedicated enzymatic or biological functions as PEA-15 knock-out (PEA-15$^{-/-}$) did not appear to affect the health and fertility in mouse models[12]. As the functions of PEA-15 are all exerted through engaging protein-protein interactions (PPIs), it is interesting to uncover how such a small, non-catalytic protein can modulate various cellular processes and bind to structurally and functionally diverse proteins in the cell, all by modifying its own phosphorylation states. In this study, we looked into the binding modes of PEA-15 with ERK2, a typical MAP kinase protein responsible for cell-cycle entry and cell proliferation[22], and FADD, an adapter protein to facilitate the association of DISC and promote the activation of initiator caspase-8 for extracellular death-ligand induced apoptosis[18].

ERK2 and FADD do not share any sequence or structural homology, and they perform very distinct biological functions in the cell. The cellular pathways they each involved do not seem to overlap. Structurally, ERK2 has typical kinase fold, with a small N-lobe composed of a five-stranded antiparallel β-sheet and containing the ATP-binding P-loop, and a large C-lobe with six conserved α-helical segments and the catalytic loop containing four short conserved β strands[23]. FADD is a death superfamily protein and is composed of an N-terminal DED and a C-terminal DD[18], both having a six-helix bundled fold but differing in intermolecular interactions[19]. They both, however, bind to PEA-15 of proper phosphorylation states. When engaged in binding, PEA-15 utilizes both its DED and the C-terminal tail to interact with partner protein through electrostatic interactions. The main binding surface on PEA-15 DED is helices α5 and α6, which is negatively charged, while the surfaces of ERK2 DEF docking site and FADD helices α1 and α6 of its DED are both positively charged. PEA-15 uses the same binding surface on the DED to engage both ERK2 and FADD in the interactions. The *in vivo* binding specificity is determined by the phosphorylation states of the two serine residues on PEA-15 C-terminal tail. When unphosphorylated, the C-terminal tail appears to be more positively charged due to the basic lysine residues towards the end of the tail. This positively charged tail will preferably interact with the negative patch of ERK2 DRS. When the C-terminal tail is phosphorylated, particularly at Ser-116, it dramatically changes the charge distribution on the tail, making it significantly more negatively charged. The change of the electrostatic property on the tail promotes the preferential binding to the positive patch on the FADD surface of helix α3 of DED. To our knowledge, this study is the first attempt to explain the phosphorylation dependent binding specificity of PEA-15.

In this MD study, together with our previous NMR studies[7,17,24], we pointed to a very flexible DED in PEA-15. PEA-15 DED adopts different conformations depending on its phosphorylation and binding status, and is allosterically controlled by its intrinsically disordered C-terminal tail. When the C-terminal tail is recognized by ERK2 DRS, the DED modulates its conformation, including the allosteric exposure of α5/α6 binding surface and relaxation of α3 to facilitate its interaction with the DEF docking site on ERK2. On the other hand, when the C-terminal tail serine residues are phosphorylated, it allosterically modulates DED conformation to prepare it to engage in DED-DED interactions. When it comes to bind with FADD, little conformational change is needed to form the complex.

This simulated PEA-15pp/FADD model agrees well with our initial NMR assessment on the complex, which demonstrated that the phosphorylation of PEA-15 C-terminal serine residues significantly modulate DED conformation, while binding to FADD does not seem to induce additional conformational change of PEA-15pp[17]. In an effort to partially assign the NMR spectra of PEA-15 S104D/S116D double mutant (PEA-15DD), mimicking the doubly phosphorylated state and having similar *in vivo* effects and binding specificity to FADD[25], we identify that the residues experiencing the most chemical shift perturbations between the free PEA-15DD and the FADD-bound form are mostly located on helices α5 and α6, including Arg-71, which engages in direct interactions with FADD. Other residues exhibiting significant shifts upon FADD binding include H52, I66, F67, I69, S70, and R72 on the DED, and Q114, D116 (mutated from serine to mimic phosphorylation and involved in FADD binding), and E117 on the C-terminal tail (Supplementary Figure S9).

On almost all DED-containing proteins, a prominent surface feature, termed charge-triad, consisting of three charged residues, D/E-RxDL (first charged residue can be either D or E, and x indicates any amino acids), can be identified to form a hydrogen-bonded and electrostatic network[19]. For PEA-15, we have illustrated the charge-triad network, D19-R72-D74 in our high-definition NMR structure[5]. However, the role of the conserved charge-triad has not been determined. Although it was stipulated that D74 is involved directly in ERK2-binding, as D74A mutation caused the loss of binding capacity of PEA-15 to ERK2[4], later crystal structures[16] and NMR dynamics study[7] both rejected such hypothesis, and we proposed that the charge-triad, through its hydrogen-bonded network, to facilitate conformational change at DED by reducing transition energy between free- and bound-conformations. The current MD simulations confirmed our hypothesis. In free-form PEA-15, D19 is hydrogen-bonded to R72, while in the ERK2-bound form, R72 is hydrogen-bonded to D74, making the switch between free- and bound-conformation swiftly. For the PEA-15pp/FADD complex, the same trend seems to hold. D19-R72 interaction dominates in the free PEA-15pp, while R72-D74 interaction is more prevalent in the bound form. D74A mutation will disrupt the interaction between R72 and D74, which is essential in complex formation. As we pointed out earlier, other surface polar interactions on PEA-15 also contribute to the conformational transition by lowering the transition energies.

Another significant finding in this study is that FADD undergoes a large conformational change upon interaction with PEA-15pp, involving a complete reorientation of the DD relative to the DED. This reorientation between the two domains has significant implication in the DISC formation in responding extracellular apoptotic signals. However, the understanding of the DISC association and the activation of initiator caspase-8 is limited by the lack of a complete DISC structural model. Two crystal structures have been reported for the complexes formed between the DD of the death receptor Fas, and the DD of the adaptor protein FADD, with PDB IDs 3EZQ[26] and 3OQ9[27]. The asymmetric oligomeric DD assembly formed between mouse Fas and human FADD DDs (3OQ9) revealed at least three types of binding interfaces in the association of DD complexes, reflecting the complexity of maintaining an intricate balance between the regulatory threshold and responsive sensitivity in triggering apoptosis[27]. The tetrameric human Fas-FADD DD complex displayed intriguing new features, in which an elongated new

stem helix is formed in place of helices α5 and α6, and an additional C-helix is formed in the C-terminus of Fas DD[26]. The stem helix and the C-helix may promote the association of Fas and formation of a regulatory bridge between Fas molecules. Another effect of shifting helix 6 and fusing with helix 5 to form the stem helix is to expose a hydrophobic patch between helices α1 and α5 of Fas DD to interact with helices α1 and α6 of FADD DD. This crystal structure implies that relative repositioning of the two domains of FADD seems to be necessary to expose caspase-8 binding surface, and to avoid the steric clash with the newly formed C-helix of Fas. Our MD simulation of PEA-15pp/FADD complex provides initial evidence of the repositioning of FADD DED relative to DD, shifting the binding surface at helices 1 and 6 for DED-DED interaction away from clashing with the Fas stem helix and C-helix. The FADD DD conformation in our simulated complex structure agrees very well with the crystal structure 3EZQ, with a backbone RMSD of 1.610 Å. The rotation of DED relative to DD makes the bound PEA-15 DED, particularly helix α6, to avoid the steric hinderance with the stem helix or the C-helix of Fas DD (Fig. 7A). As a comparison, the NMR structure of full-length FADD (2GF5) had a backbone RMSD of 4.334 Å for the DD with crystal structure 3EZQ, and if we assume PEA-15 binding at the same surface at helices α1 and α6 of FADD DED, significant clashing between PEA-15 helix α6 and the stem helix and C-helix can be detected (Fig. 7B). Since it is reasonable to assume that PEA-15 DED and caspase-8 DED may bind to the same surface of FADD DED, the relative reorientation between the two domains of FADD will be crucial in recruiting caspase-8 to the DISC. Our MD model provides an important insight into the DISC formation and caspase-8 activation.

Methods

Construction of initial free-form and complex models

The PEA-15 in its free-form was constructed from the NMR structure, PDB ID 2LS7[5], by adding the C-terminal tails residues 91–130 as random coil using the comparative protein structure modeling program Modeller[28–31]. The PEA-15pp model was constructed from the final simulated structure of the unmodified PEA-15 by adding phosphoryl group to each of Ser-104 and Ser-116 residue using the posttranslational modification plugin, PyTMS[32], for the molecular graphics system PyMOL (Schrödinger, LLC., New York, NY).

The complex model between PEA-15 and ERK2 was constructed from the crystal structure of the complex, PDB ID 4IZ5[16]. The missing residues in the PEA-15 chain of the crystal structure were rebuilt from the Rosetta model of ERK2-bound PEA-15, PDB ID 6P6C[17], using the Modeller program. The T185E mutation in the ERK2 of the crystal structure was also changed back to a threonine using Modeller.

As there are currently no PEA-15 and FADD complex structure, the complex model between PEA-15pp and FADD was constructed using the final simulated PEA-15pp structure docked with the NMR structure of intact FADD, PDB ID 2GF5[18], using online SwarmDock Server[33–35]. Among the 10 best docking models generated by the Server, the model selected for further MD simulations matches best with the NMR

chemical shift perturbation data, which is indicative of protein-protein binding interface between the two proteins (Supplementary Figure S7).

MD simulation protocols

All-atom MD simulations with explicit solvent were performed with the parallel molecular dynamics package GROMACS[36–42] with CUDA-based GPU acceleration on an Exxact workstation equipped with two Nvidia Tesla V100 GPUs running CentOS 8 and GROMACS version 2020-3. The simulation timescale was 50 ns for both the full-length, unmodified PEA-15 model and the doubly phosphorylated PEA-15pp model, and 150 ns for the two complexes of PEA-15/ERK and PEA-15pp/FADD. All simulations were conducted at neutral pH, 300 K, and 1 atm. CHARMM36 force field[43] was utilized for all protein parameters.

All starting protein structures were solvated in a cubic box with boundaries extended at least 1.0 nm in all directions from the protein molecules, and filled with TIP3P water molecules and appropriate number of counter ions (either Na^+ or Cl^-) to neutralize the total charge of the system. Energy minimization was performed using steepest descent algorithm with convergence on $F_{max} < 1000$ kJ mol^{-1} nm^{-1}. Equilibration was conducted in two phased, 100 ps under *NVT* (constant number of particles, volume, and temperature) and 100 ps under *NPT* (constant number of particles, pressure, and temperature) ensembles, while restraining atomic position. The coupling time constant was set to 0.1 ps for the equilibration, and periodic boundary conditions were applied with constant temperature of 300 K and constant pressure of 1 atm. Heavy atom bond lengths were constrained using Linear Constraint Solver (LINCS) algorithm. For the production MD run, both Coulomb and van der Waals interactions were truncated at 1.2 nm, with Particle Mesh Ewald (PME) summation method for the long-range electrostatic interactions. Production runs (50 ns for free-form proteins and 150 ns for protein complexes with a timestep of 2 fs) were performed upon the equilibrated system using CHARMM36 force field and the leap-frog algorithm utilizing both NVidia Tesla V100 GPUs for acceleration. Snapshots of conformations were collected at every 100 ps.

Analysis of MD results

MD trajectories were analyzed using GROMACS tools. Secondary structural content was determined using program DSSP[44]. Root-mean-square deviation (RMSD) from the starting structure and root-mean-square fluctuation (RMSF) to highlight highly flexible regions were calculated using the Cartesian coordinates of the Cα atoms. The RMSD for free-form PEA-15 proteins stabilized at around 30 ns due to the flexible C-terminal tail, and the final 20-ns trajectories were utilized for the analysis. The RMSD for the complex structures stabilized at around 100 ns, and the last 50-ns trajectories were included in the analysis. Various intramolecular and intermolecular hydrogen bonding distances were calculated to map out the polar surface interaction network on PEA-15 and the intermolecular interactions that stabilize the complex structures.

Calculation of electrostatic potential surfaces

The EPS each individual protein in the PEA-15/ERK2 and PEA-15pp/FADD complexes were calculated with the APBS (Adaptive Poisson-Boltzmann Solver) method[45] implemented in the Maestro program (Schrödinger, LLC, New York, NY). This method creates a molecular surface and colors the Poisson-Boltzmann (PB) potential onto the protein surface. Negative potential is colored by red and positive potential colored by blue. A solvent dielectric constant of 80 and a solvent radius of 1.4 Å were used in the calculations.

Molecular visualization

All molecular models were visualized and produced using either PyMOL or Maestro, including structural superposition and comparison, distance and hydrogen-bonding analysis, protein-protein interface analysis, and EPS analysis.

Declarations

Acknowledgement

This research was funded by the National Institute on Drug Abuse (NIDA) of the National Institutes of Health (NIH), grant number R21DA046223. We also thank Dr. John Grew of New Jersey City University for supporting student research and the acquisition of computational hardware with his grants, US Education Department Title III Part F HSI-STEM Grant # P031C160155, and US Education Department Title V DHSI Grant # P031S200124.

Author Contributions

J.I. performed most of the experiments, conducted structural analysis and data interpretation, and participated in drafting the manuscript. J.H. conducted part of data analysis and interpretation and participated in revising the manuscript. Y.W. conceived and designed the experiments, trained students in performing the experiments, conducted data analysis and interpretation, drafted and revised the manuscript, and secured external funding for the research. All authors discussed the results and commented on the manuscript.

Competing Interests

The authors declare no competing interests.

References

1. Wei, Y. On the Quest of Cellular Functions of PEA-15 and the Therapeutic Opportunities. *Pharmaceuticals (Basel, Switzerland)*, **8**, 455–473 https://doi.org/10.3390/ph8030455 (2015).
2. Araujo, H., Danziger, N., Cordier, J., Glowinski, J. & Chneiweiss, H. Characterization of PEA-15, a major substrate for protein kinase C in astrocytes. *The Journal of biological chemistry*, **268**, 5911–5920 (1993).
3. Kirsch, T. *et al.* Cloning, high-yield expression in Escherichia coli, and purification of biologically active HIV-1 Tat protein. *Protein Expr Purif*, **8**, 75–84 https://doi.org/10.1006/prep.1996.0076 (1996).
4. Hill, J. M., Vaidyanathan, H., Ramos, J. W., Ginsberg, M. H. & Werner, M. H. Recognition of ERK MAP kinase by PEA-15 reveals a common docking site within the death domain and death effector domain. *EMBO J*, **21**, 6494–6504 https://doi.org/10.1093/emboj/cdf641 (2002).
5. Twomey, E. C. & Wei, Y. High-definition NMR structure of PED/PEA-15 death effector domain reveals details of key polar side chain interactions. *Biochemical and Biophysical Research Communications*, **424**, 141–146 https://doi.org/10.1016/j.bbrc.2012.06.091 (2012).
6. Kaoud, T. S. *et al.* Activated ERK2 Is a Monomer in Vitro with or without Divalent Cations and When Complexed to the Cytoplasmic Scaffold PEA-15., **50**, 4568–4578 https://doi.org/10.1021/bi200202y (2011).
7. Twomey, E. C., Cordasco, D. F. & Wei, Y. Profound conformational changes of PED/PEA-15 in ERK2 complex revealed by NMR backbone dynamics. *Biochimica et Biophysica Acta (BBA) - Proteins and Proteomics*, **1824**, 1382–1393 https://doi.org/10.1016/j.bbapap.2012.07.001 (2012).
8. Kubes, M., Cordier, J., Glowinski, J., Girault, J. A. & Chneiweiss, H. Endothelin Induces a Calcium-Dependent Phosphorylation of PEA-15 in Intact Astrocytes: Identification of Ser104 and Ser116 Phosphorylated, Respectively, by Protein Kinase C and Calcium/Calmodulin Kinase II In Vitro. *Journal of Neurochemistry*, **71**, 1307–1314 https://doi.org/10.1046/j.1471-4159.1998.71031307.x (1998).
9. Trencia, A. *et al.* Protein Kinase B/Akt Binds and Phosphorylates PED/PEA-15, Stabilizing Its Antiapoptotic Action. *Mol. Cell. Biol*, **23**, 4511–4521 https://doi.org/10.1128/mcb.23.13.4511-4521.2003 (2003).
10. Formstecher, E. *et al.* PEA-15 Mediates Cytoplasmic Sequestration of ERK MAP Kinase. *Dev. Cell*, **1**, 239–250 https://doi.org/10.1016/s1534-5807(01)00035-1 (2001).
11. Condorelli, G. *et al.* PED/PEA-15: an anti-apoptotic molecule that regulates FAS/TNFR1-induced apoptosis., **18**, 4409–4415 https://doi.org/10.1038/sj.onc.1202831 (1999).
12. Kitsberg, D. *et al.* Knock-Out of the Neural Death Effector Domain Protein PEA-15 Demonstrates That Its Expression Protects Astrocytes from TNFα-Induced Apoptosis. *The Journal of Neuroscience*, **19**, 8244–8251 (1999).
13. Hao, C. *et al.* Induction and Intracellular Regulation of Tumor Necrosis Factor-related Apoptosis-inducing Ligand (TRAIL) Mediated Apotosis in Human Malignant Glioma Cells. *Cancer Res*, **61**, 1162–1170 (2001).
14. Renganathan, H., Vaidyanathan, H., Knapinska, A. & Ramos, J. W. Phosphorylation of PEA-15 switches its binding specificity from ERK/MAPK to FADD. *Biochem. J*, **390**, 729–735

https://doi.org/10.1042/bj20050378 (2005).

15. Sulzmaier, F., Opoku-Ansah, J. & Ramos, J. W. Phosphorylation is the switch that turns PEA-15 from tumor suppressor to tumor promoter. *Small GTPases*, **3**, 173–177 https://doi.org/10.4161/sgtp.20021 (2012).
16. Mace, P. D. *et al.* Structure of ERK2 bound to PEA-15 reveals a mechanism for rapid release of activated MAPK. *Nat Commun*, **4**, 1681 https://doi.org/10.1038/ncomms2687 (2013).
17. Crespo-Flores, S. L., Cabezas, A., Hassan, S. & Wei, Y. PEA-15 C-Terminal Tail Allosterically Modulates Death-Effector Domain Conformation and Facilitates Protein–Protein Interactions. *International Journal of Molecular Sciences*, **20**, 3335 https://doi.org/10.3390/ijms20133335 (2019).
18. Carrington, P. E. *et al.* The Structure of FADD and Its Mode of Interaction with Procaspase-8. *Mol. Cell*, **22**, 599–610 https://doi.org/10.1016/j.molcel.2006.04.018 (2006).
19. Park, H. H. *et al.* The Death Domain Superfamily in Intracellular Signaling of Apoptosis and Inflammation. *Annual Review of Immunology*, **25**, 561–586 https://doi.org/10.1146/annurev.immunol.25.022106.141656 (2007).
20. Callaway, K., Rainey, M. A. & Dalby, K. N. Quantifying ERK2-protein interactions by fluorescence anisotropy: PEA-15 inhibits ERK2 by blocking the binding of DEJL domains. *Biochimica et Biophysica Acta (BBA) - Proteins & Proteomics*, **1754**, 316–323 https://doi.org/10.1016/j.bbapap.2005.11.002 (2005).
21. Callaway, K., Abramczyk, O., Martin, L. & Dalby, K. N. The Anti-Apoptotic Protein PEA-15 Is a Tight Binding Inhibitor of ERK1 and ERK2, Which Blocks Docking Interactions at the D-Recruitment Site†., **46**, 9187–9198 https://doi.org/10.1021/bi700206u (2007).
22. Roskoski, R. Jr. ERK1/2 MAP kinases: structure, function, and regulation. *Pharmacol Res*, **66**, 105–143 https://doi.org/10.1016/j.phrs.2012.04.005 (2012).
23. Zhang, F., Robbins, D. J., Cobb, M. H. & Goldsmith, E. J. Crystallization and preliminary X-ray studies of extracellular signal-regulated kinase-2/MAP kinase with an incorporated His-tag. *J Mol Biol*, **233**, 550–552 https://doi.org/10.1006/jmbi.1993.1532 (1993).
24. Twomey, E. C., Cordasco, D. F., Kozuch, S. D. & Wei, Y. Substantial Conformational Change Mediated by Charge-Triad Residues of the Death Effector Domain in Protein-Protein Interactions. *PLoS ONE*, **8**, e83421 https://doi.org/10.1371/journal.pone.0083421 (2013).
25. Lee, J. *et al.* PEA-15 unphosphorylated at both serine 104 and serine 116 inhibits ovarian cancer cell tumorigenicity and progression through blocking beta-catenin. *Oncogenesis*, **1**, e22 https://doi.org/10.1038/oncsis.2012.22 (2012).
26. Scott, F. L. *et al.* The Fas-FADD death domain complex structure unravels signalling by receptor clustering. *Nature*, **457**, 1019–1022 https://doi.org/10.1038/nature07606 (2009).
27. Wang, L. *et al.* The Fas-FADD death domain complex structure reveals the basis of DISC assembly and disease mutations. *Nat Struct Mol Biol*, **17**, 1324–1329 https://doi.org/10.1038/nsmb.1920 (2010).

28. Webb, B. & Sali, A. Comparative Protein Structure Modeling Using MODELLER. *Curr Protoc Bioinformatics*, **54**, https://doi.org/5.6.1–5.6.37 (2016).
29. Martí-Renom, M. A. *et al.* Comparative protein structure modeling of genes and genomes. *Annu Rev Biophys Biomol Struct*, **29**, 291–325 https://doi.org/10.1146/annurev.biophys.29.1.291 (2000).
30. Sali, A. & Blundell, T. L. Comparative protein modelling by satisfaction of spatial restraints. *J Mol Biol*, **234**, 779–815 https://doi.org/10.1006/jmbi.1993.1626 (1993).
31. Fiser, A., Do, R. K. & Sali, A. Modeling of loops in protein structures. *Protein Sci*, **9**, 1753–1773 https://doi.org/10.1110/ps.9.9.1753 (2000).
32. Warnecke, A., Sandalova, T., Achour, A. & Harris, R. A. PyTMs: a useful PyMOL plugin for modeling common post-translational modifications. *BMC Bioinformatics*, **15**, 370 https://doi.org/10.1186/s12859-014-0370-6 (2014).
33. Torchala, M., Moal, I. H., Chaleil, R. A. G., Fernandez-Recio, J. & Bates, P. A. SwarmDock: a server for flexible protein–protein docking., **29**, 807–809 https://doi.org/10.1093/bioinformatics/btt038 (2013).
34. Torchala, M., Moal, I. H., Chaleil, R. A. G., Agius, R. & Bates, P. A. A Markov-chain model description of binding funnels to enhance the ranking of docked solutions. *Proteins: Structure, Function, and Bioinformatics*, **81**, 2143–2149 https://doi.org/10.1002/prot.24369 (2013).
35. Torchala, M. & Bates, P. A. in Protein Structure Prediction (ed Daisuke Kihara) 181–197(Springer New York, 2014).
36. Berendsen, H. J. C., van der Spoel, D. & van Drunen, R. G. R. O. M. A. C. S. A message-passing parallel molecular dynamics implementation. *Comput. Phys. Commun*, **91**, 43–56 https://doi.org/10.1016/0010-4655(95)00042-E (1995).
37. Lindahl, E., Hess, B. & van der Spoel D. GROMACS 3.0: a package for molecular simulation and trajectory analysis. *Molecular modeling annual* **7**, 306–317, doi:10.1007/s008940100045 (2001).
38. Van Der Spoel, D. *et al.* Fast, flexible, and free. *Journal of Computational Chemistry 26*, **GROMACS**, 1701–1718 https://doi.org/10.1002/jcc.20291 (2005).
39. Hess, B., Kutzner, C., van der Spoel, D. & Lindahl, E. GROMACS 4: Algorithms for Highly Efficient, Load-Balanced, and Scalable Molecular Simulation. *Journal of Chemical Theory and Computation*, **4**, 435–447 https://doi.org/10.1021/ct700301q (2008).
40. Pronk, S. *et al.* GROMACS 4.5: a high-throughput and highly parallel open source molecular simulation toolkit., **29**, 845–854 https://doi.org/10.1093/bioinformatics/btt055 (2013).
41. Páll, S., Abraham, M. J., Kutzner, C., Hess, B. & Lindahl E. 3–27 (Springer International Publishing).
42. Abraham, M. J. *et al.* GROMACS: High performance molecular simulations through multi-level parallelism from laptops to supercomputers. *SoftwareX* **1–2**, 19–25, doi:https://doi.org/10.1016/j.softx.2015.06.001 (2015).
43. Brooks, B. R. *et al.* CHARMM: the biomolecular simulation program. *Journal of computational chemistry*, **30**, 1545–1614 https://doi.org/10.1002/jcc.21287 (2009).

44. Touw, W. G. *et al.* A series of PDB-related databanks for everyday needs. *Nucleic acids research*, **43**, D364–D368 https://doi.org/10.1093/nar/gku1028 (2015).
45. Jurrus, E. *et al.* Improvements to the APBS biomolecular solvation software suite. *Protein Sci*, **27**, 112–128 https://doi.org/10.1002/pro.3280 (2018).

Figures

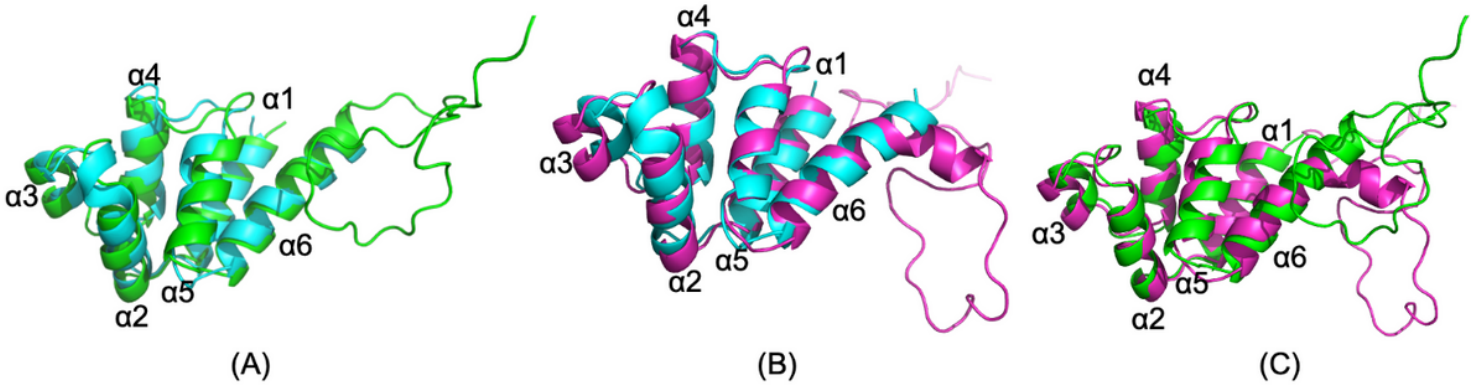

Figure 1

Superimpositions of (A) simulated free PEA-15, unphosphorylated (green) and NMR structure 2LS7 (cyan), (B) simulated free PEA-15pp, doubly phosphorylated p-S104, p-S116 (magenta) and NMR structure 2LS7 (cyan), and (C) simulated free PEA-15, unphosphorylated (green) and simulated PEA-15pp, doubly phosphorylated (magenta). Note that NMR structure 2LS7 contains only DED structure without the C-terminal tail. The simulated structure of unphosphorylated PEA-15 closely resembles the experimental NMR structure for the DED (RMSD 1.499 Å), while the simulated phosphorylated PEA-15pp has very different conformation from the NMR structure (RMSD 2.027 Å). The simulated unphosphorylated PEA-15 and phosphorylated PEA-15pp also display conformational differences, with RMSD of 1.994 Å.

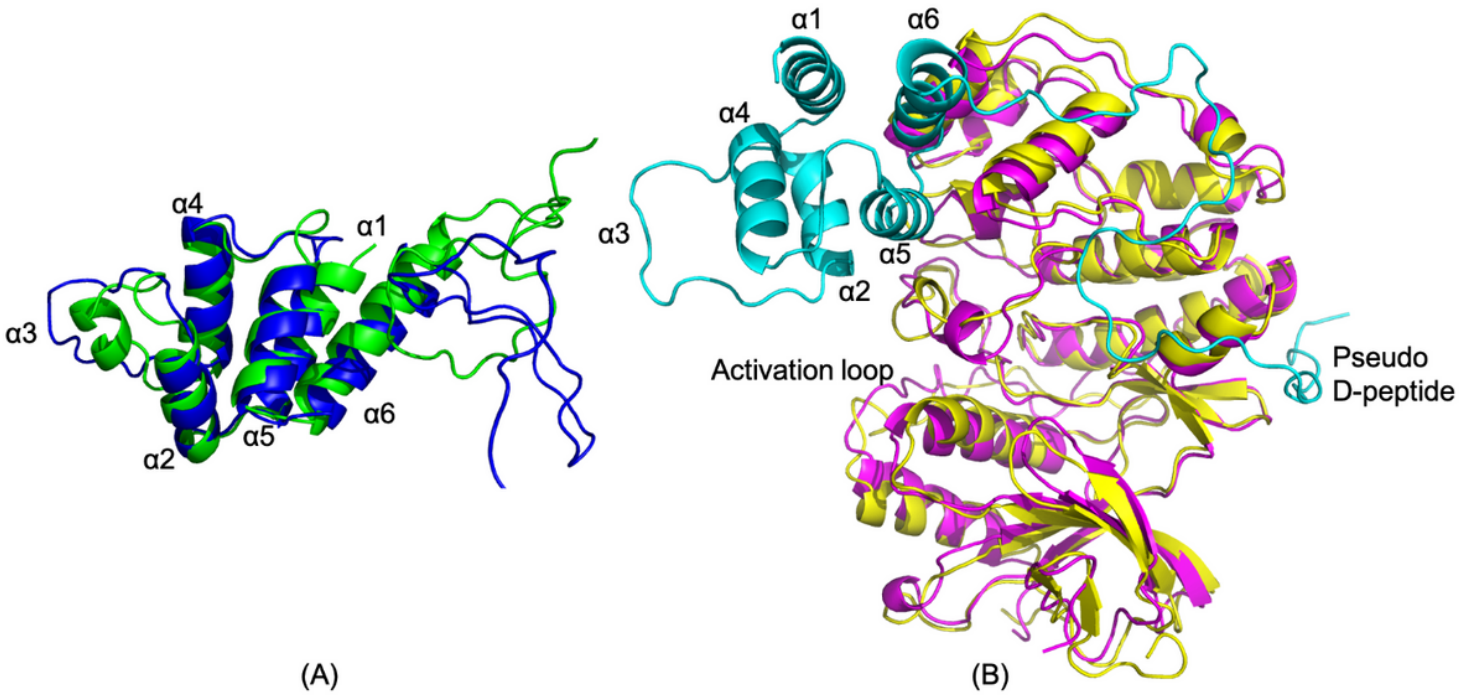

Figure 2

Simulated complex structure of PEA-15/ERK2. (A) PEA-15 in the complex (green) is superimposed with its free form (blue) with the RMSD 2.734 Å for the DED. Helix α3 is uncoiled and shifts in α2 and α4 can also be observed. (B) ERK2 in the complex is superimposed with crystal structure of 4IZ5 with the RMSD 2.002 Å. The overall backbone of ERK2 does not show any significant difference between the simulated and crystal structure.

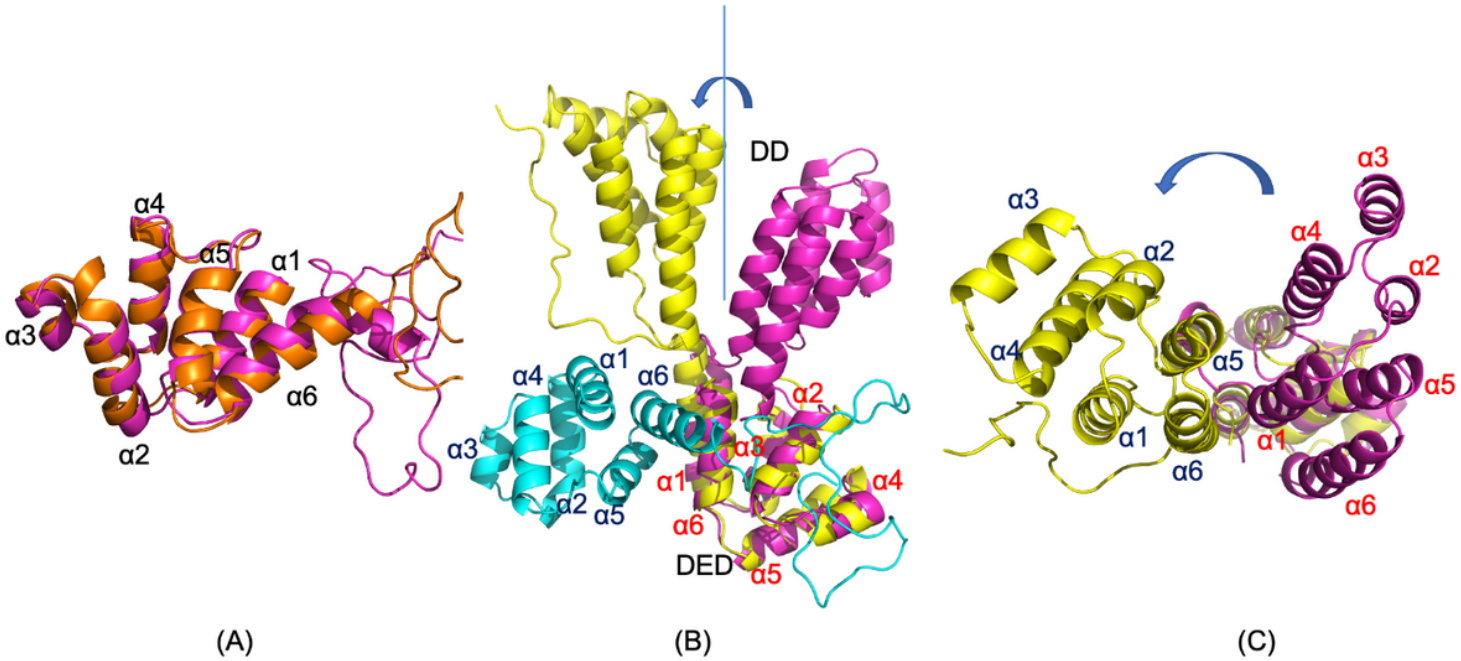

Figure 3

Simulated complex structure of PEA-15pp/FADD. (A) PEA-15pp in the complex (orange) is superimposed with free-form PEA-15pp (magenta) with the RMSD of 0.803 Å before the kink on helix α6. There is no significant conformational change between the free and bound form. (B) FADD in the complex (yellow) is superimposed with NMR structure of intact FADD, 2GF5 (meganta), over DED residues (RMSD 2.118 Å). PEA-15pp in the complex is colored cyan. DED-DED interaction in the complex is orthogonal in directions. The FADD DD in the complex rotated about 90° from the free form around the linker between the two domains. (C) same as (B), but observed from the top of FADD DD to illustrate the relative positions of the six helices on DD. PEA-15pp is not shown for clarity.

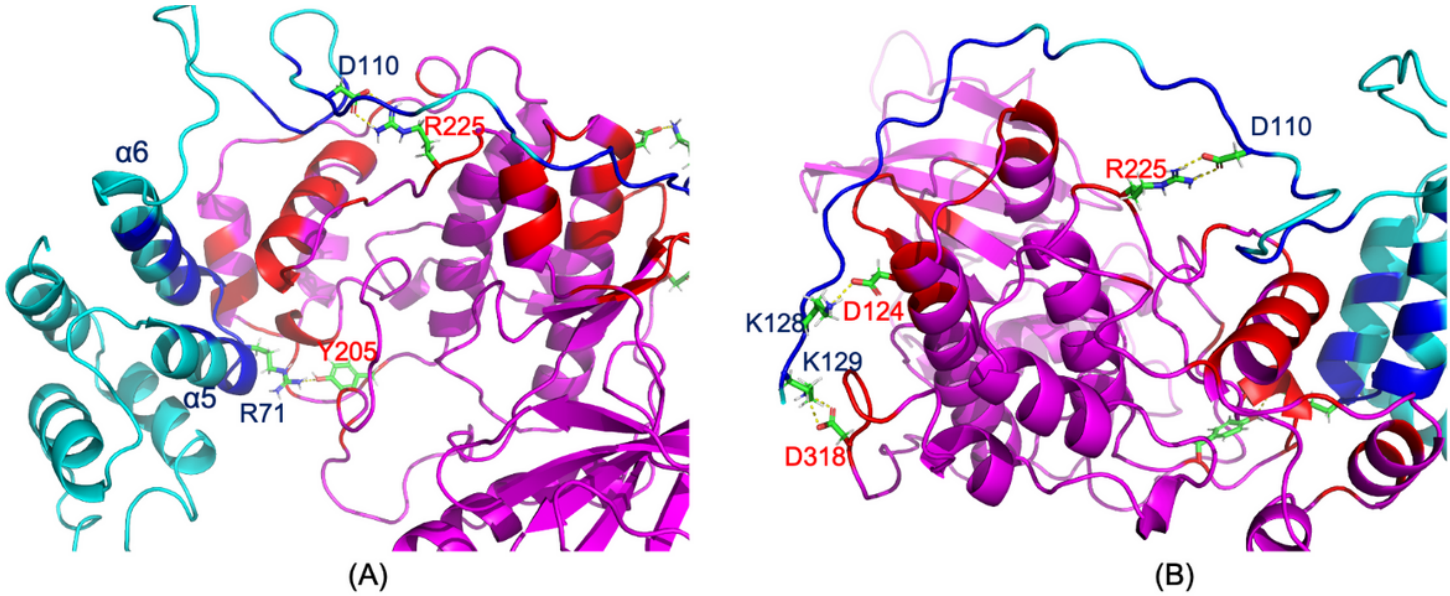

Figure 4

Binding interfaces in the simulated PEA-15/ERK2 complex. PEA-15 is shown in cyan and ERK2 in magenta. Interface residues on PEA-15 are colored in dark blue, and residues on ERK2 are colored in red. (A) Interface between PEA-15 DED and ERK2 DEF docking site. PEA-15 interacts with ERK2 with its helices α5/α6, including a direct interaction between PEA-15 R71 and ERK2 Y205, in consistent with crystal structure 4IZ5. (B) Interface between PEA-15 C-terminal tail and ERK2 D-peptide binding site, including interactions between PEA-15 K128 and ERK2 D124 and PEA-15 K129 and ERK2 D318. Another interaction can be observed is between PEA-15 D110 and ERK2 R225. There are no direct interactions between either phosphorylation sites, S104 and S116, and ERK2 residues.

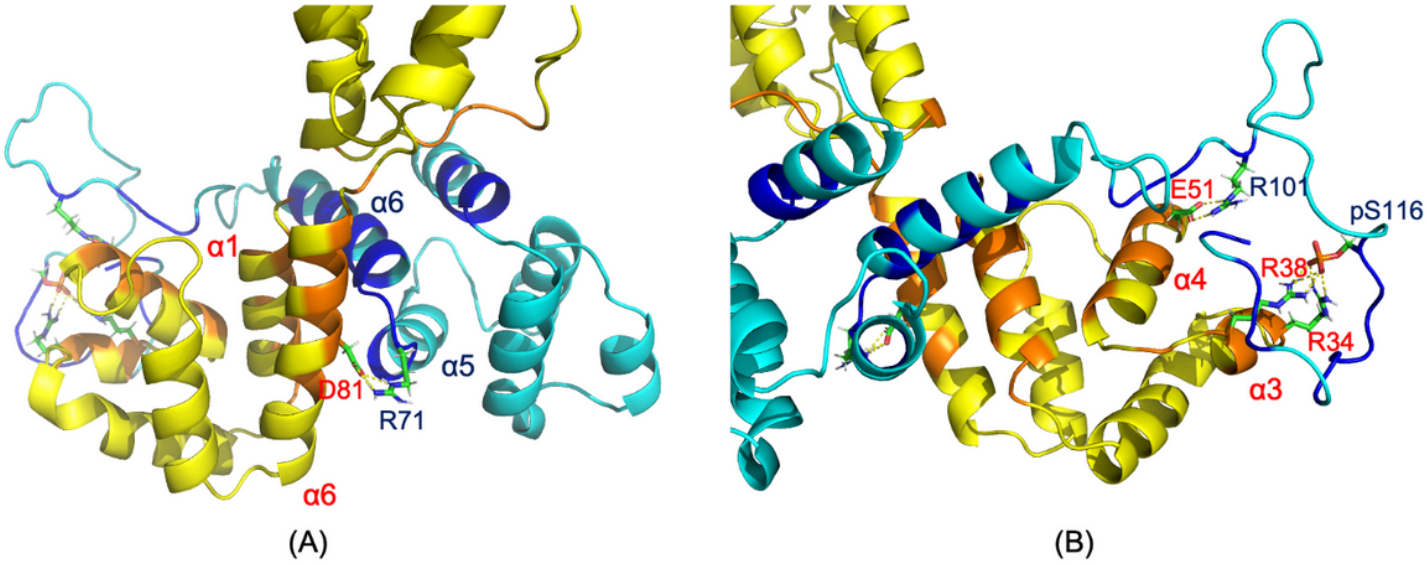

Figure 5

Binding interfaces in the simulated PEA-15pp/FADD complex. PEA-15pp is shown in cyan and FADD is shown in yellow. Interface residues on PEA-15 are colored in blue and residues on FADD are colored in orange. (A) DED-DED interface between PEA-15pp α5/α6 and FADD α1/α6, including direct interaction between PEA-15 R71 and FADD D81. (B) Interface between PEA-15pp C-terminal tail and FADD helices α3/α4, including direct interactions between PEA-15 R101 and FADD E51, and the strong interactions between PEA-15pp p-S116 and FADD R38 and R38.

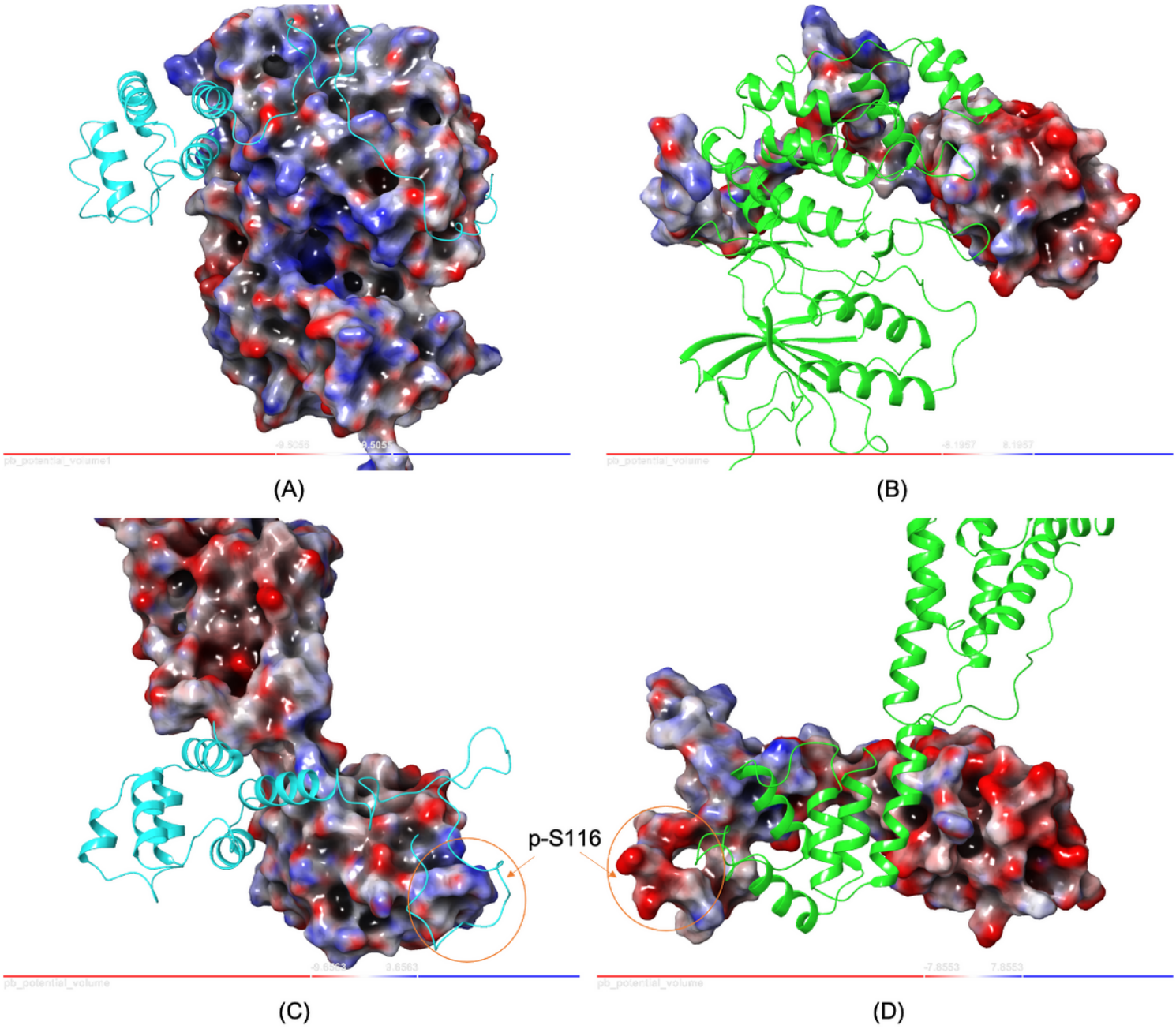

Figure 6

Poisson-Boltzmann Electrostatic Potential Surfaces (PB EPS) of PEA-15/ERK2 (A and B) and PEA-15pp/FADD (C and D) complexes. (A) ERK2 is shown as EPS and PEA-15 as ribbon in cyan. (B) PEA-15 is shown as EPS and ERK2 as ribbon in green. The view in (B) is rotated 180° from (A). (C) FADD is shown as EPS and PEA-15pp as ribbon in cyan. (D) PEA-15pp is shown as EPS and FADD as ribbon in green. The view in (D) is rotated 180° from (C). On the EPS, negative charge is represented as red and positive charge as blue. Protein-protein interactions are largely electrostatic in nature. Note that in PEA-15pp/FADD interaction, there is a strong electrostatic interaction between negatively charged p-S116 on PEA-15pp and the positive patch formed by R34 and R38 on FADD, which determines the binding specificity of PEA-15.

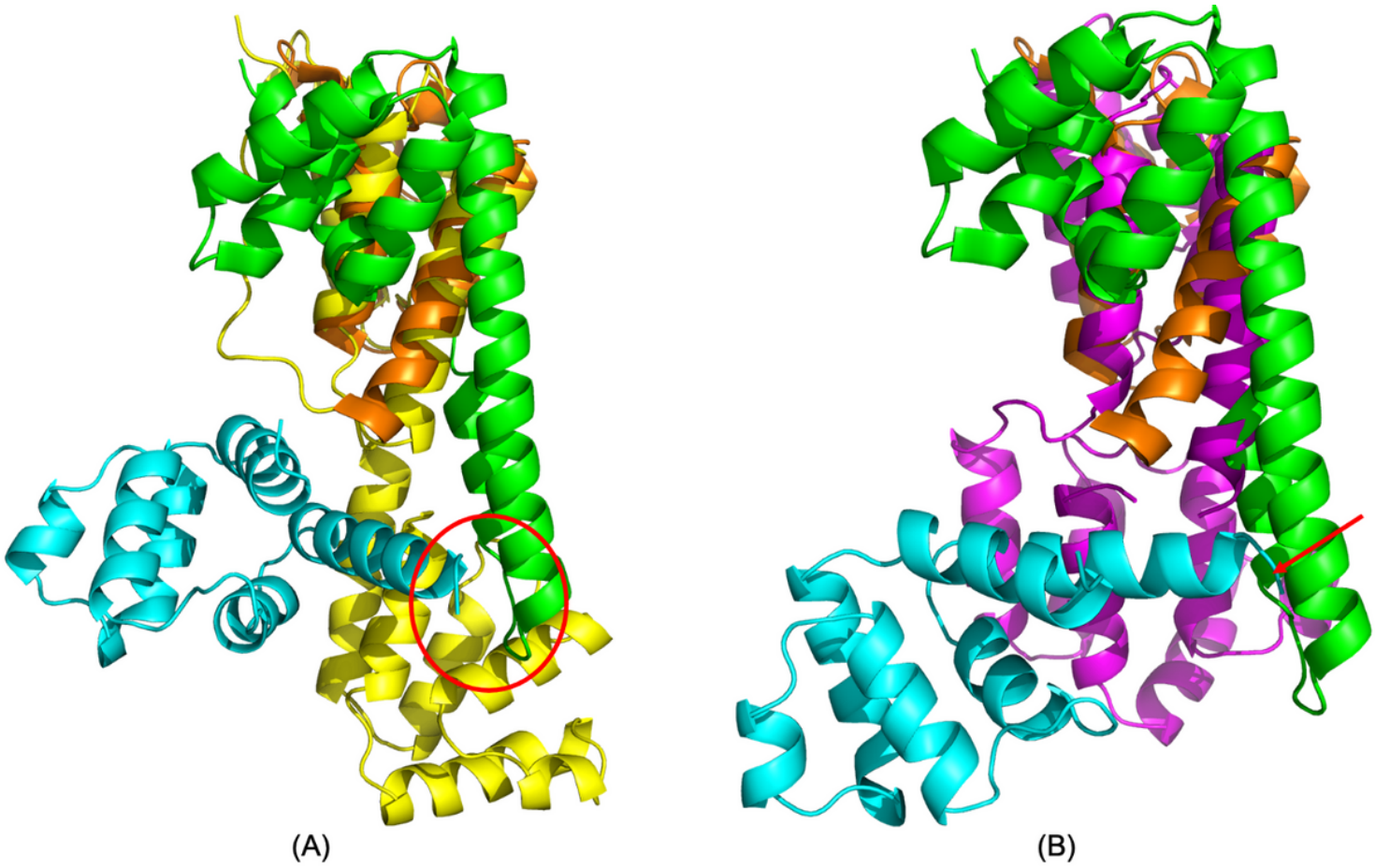

Figure 7

(A) Overlay of simulated PEA-15pp/FADD complex (PEA-15pp in cyan and FADD in yellow) onto Fas-FADD DD complex crystal structure (Fas DD in green and FADD DD in orange), 3EQZ, over FADD DD residues. The simulated FADD DD structure matches very well with the crystal structure with the RMSD of 1.610 Å. (B) Overlay of NMR structure of intact FADD (magenta), 2GF5, onto Fas-FDD DD complex crystal structure (Fas DD in green and FADD DD in orange), 3EQZ over FADD DD residues. The RMSD between FADD DD is 4.334 Å, indicating a conformational change in the DD upon complex formation. Assuming PEA-15pp binds to the same position of FADD DED (shown in cyan), its helix α6 will clash with the newly formed stem helix and C-helix on Fas DD (indicated by red arrow). In our simulated structure, however, due to the relative repositioning FADD DD and DED, the bound PEA-15 DED can avoid such steric hinderance, indicated as red circle in (A). The C-terminal tail of PEA-15pp is not shown for clarity.

Supplementary Files

This is a list of supplementary files associated with this preprint. Click to download.

- PEA15MDsimulationoninteractionsSupplementaryInformation.pdf